Click Here for Full Article

Broadband simulations for M_w 7.8 southern San Andreas earthquakes: Ground motion sensitivity to rupture speed

Robert W. Graves,[1] Brad T. Aagaard,[2] Kenneth W. Hudnut,[3] Lisa M. Star,[4] Jonathan P. Stewart,[4] and Thomas H. Jordan[5]

Received 20 August 2008; revised 6 October 2008; accepted 9 October 2008; published 20 November 2008.

[1] Using the high-performance computing resources of the Southern California Earthquake Center, we simulate broadband (0–10 Hz) ground motions for three M_w 7.8 rupture scenarios of the southern San Andreas fault. The scenarios incorporate a kinematic rupture description with the average rupture speed along the large slip portions of the fault set at 0.96, 0.89, and 0.84 times the local shear wave velocity. Consistent with previous simulations, a southern hypocenter efficiently channels energy into the Los Angeles region along the string of basins south of the San Gabriel Mountains. However, we find the basin ground motion levels are quite sensitive to the prescribed rupture speed, with peak ground velocities at some sites varying by over a factor of two for variations in average rupture speed of about 15%. These results have important implications for estimating seismic hazards in Southern California and emphasize the need for improved understanding of earthquake rupture processes. **Citation:** Graves, R. W., B. T. Aagaard, K. W. Hudnut, L. M. Star, J. P. Stewart, and T. H. Jordan (2008), Broadband simulations for M_w 7.8 southern San Andreas earthquakes: Ground motion sensitivity to rupture speed, *Geophys. Res. Lett.*, *35*, L22302, doi:10.1029/2008GL035750.

1. Introduction

[2] The Great Southern California ShakeOut (www.shakeout.org) is a NEHRP-coordinated, multi-hazard response exercise based on an M_w 7.8 rupture scenario of the southern San Andreas fault [*Jones et al.*, 2008]. The multi-hazard approach considers the cascade of consequences from a scenario event including casualties, damage to the built environment, and economic losses. A key component of this process is the estimation of ground shaking that will occur throughout Southern California during this event, which we have developed using a physics-based earthquake simulation methodology.

[3] The simulation approach offers several advantages over empirical ground motion prediction equations (GMPE), including explicit consideration of scenario-specific effects, such as slip distribution and hypocenter; computation of full three-component, site-specific waveforms (e.g. for the analysis of non-linear structural response); and coupling between rupture directivity and basin response in the ground motion estimation. Over the last decade, the Southern California Earthquake Center (SCEC) has developed detailed 3D models of the fault and seismic velocity structure of southern California. The simulations were computed using the SCEC Community Fault Model version 3.0 (CFM3) and the SCEC 3D Community Velocity Model (CVM4) (http://epicenter.usc.edu/cmeportal/cmodels.html).

[4] In our kinematic parameterization the rupture speed scales at a prescribed factor times the local shear wave speed. Unfortunately, the relationship between rupture speed and shear velocity is still poorly understood with both theoretical and laboratory models suggesting that a range of sustained rupture speeds from sub-shear to super-shear are possible [e.g., *Freund*, 1979; *Rosakis et al.*, 1999]. *Aagaard and Heaton* [2004] assessed the sensitivity of ground motions to rupture speed using a kinematic prescription on planar faults in a 1D structure and found ruptures propagating at or near the shear velocity produced the strongest near fault motions. Here, we extend this work by considering non-planar fault geometry and 3D velocity structure to investigate how changes in the average rupture speed impact the pattern and level of ground motions, and how these motions couple with the 3D basins of this region.

2. Rupture Model Description

[5] The ShakeOut rupture extends 305 km along the San Andreas from Bombay Beach, on the Salton Sea, to Lake Hughes, 20 km northwest of Palmdale (Figure 1). It comprises the Coachella, San Gorgonio, San Bernardino, and South Mojave sections of the fault, for which the average paleoseismic repeat time is about 150 years [*Weldon et al.*, 2005]. The South Mojave section last ruptured in the 1857 Fort Tejon earthquake, whereas the most recent major event on the Coachella section was circa 1680 [*Sieh and Williams*, 1990].

[6] The slip distribution in the scenario blends the slip-predictable model of *Jones et al.* [2008] for length scales greater than 30 km with a random-phase model having a wavenumber-squared falloff [*Mai and Beroza*, 2002] at smaller scales. The average slip across the entire fault is about 4.6 m; however, the largest slip is concentrated along the Coachella section, which averages about 7 m of slip over the initial 70 km of the rupture. The rupture propagation speed scales linearly with relative slip at a prescribed fraction of the local shear wavespeed, V_s, consistent with spontaneous rupture models [e.g., *Day*, 1982]. In the base ShakeOut scenario, the rupture speed is set to 1.4 V_s at the point of maximum slip (16.9 m), 0.85 V_s in regions of average slip (4.6 m), and 0.20 V_s in regions of negligible

[1] URS Corporation, Pasadena, California, USA.
[2] USGS, Menlo Park, California, USA.
[3] USGS, Pasadena, California, USA.
[4] Department of Civil and Environmental Engineering, University of California, Los Angeles, California, USA.
[5] Department of Earth Sciences, University of Southern California, Los Angeles, California, USA.

Copyright 2008 by the American Geophysical Union.
0094-8276/08/2008GL035750$05.00

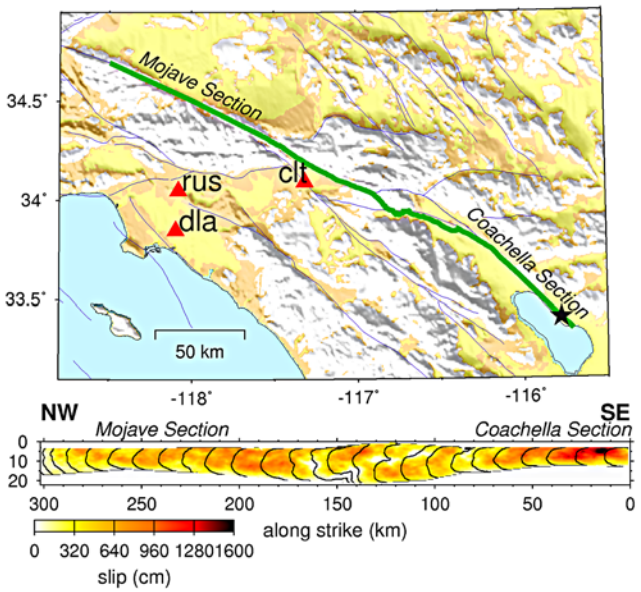

Figure 1. Map of Southern California region showing the segment of the San Andreas fault used for the shakeout scenario (green trace) and locations of selected sites discussed in text (red triangles). The base-case ShakeOut rupture model is displayed at bottom with rupture front contours shown at 4 second intervals.

slip. For the prescribed slip distribution, the rupture speed exceeds the local V_s (super-shear) over much of the initial 70 km of the fault rupture (Coachella section), with an average rupture speed of about 0.96 V_s along this section. Two additional scenarios were obtained by uniformly scaling the base case rupture speed by factors of 0.93 and 0.87, respectively. In these scenarios, the average rupture speed along the Coachella section becomes 0.89 V_s and 0.84 V_s, respectively, although super-shear rupture still occurs along the highest slip portions of the fault. Plots showing the rupture speed across the fault surface for the three scenarios are provided in the auxiliary material.[1] For all scenarios, the rupture speed was tapered by 50% over 3 km along both the top and bottom edges of the rupture, consistent with rupture propagating from regions of unstable to stable sliding. Slip initiation times were determined from the rupture speed distribution by tracing the rupture front away from the hypocenter assuming locally circular wave fronts.

[7] The slip time function is a Brune pulse with a rise time proportional to the square root of slip. The rise time increases linearly over 5 km along the top and bottom edges of the rupture, similar to the decrease in rupture speed [e.g., *Aagaard et al.*, 2008]. This kinematic source model was mapped onto the CFM3 fault surface representation, which includes variations in strike, dip, and fault width.

3. Simulation Methodology

[8] The broadband (0–10 Hz) ground motion simulations use the hybrid procedure of *Graves and Pitarka* [2004], which combines a 3D deterministic approach at low frequencies (<1 Hz) with a semi-stochastic approach at high frequencies (>1 Hz). The method has been validated using broadband data from several earthquakes, including the 1989 Loma Prieta and 1994 Northridge events. The low-frequency motions were calculated using a 3D visco-elastic, finite-difference algorithm [*Graves*, 1996; *Day and Bradley*, 2001] by embedding the full kinematic rupture description in the CVM4 velocity structure. Anelastic attenuation was modeled using the relations $Q_s = 50V_s$ (for V_s in km/s) and $Q_p = 2Q_s$. In the near surface layers, we set the minimum shear velocity at 0.62 km/s, which dictated a grid size of 0.125 km for the finite-difference calculation.

[9] We performed the simulations at USC's High Performance Computing Center, which were made available through the SCEC Community Modeling Environment [*Jordan and Maechling*, 2003]. Low-frequency simulations for the base scenario were also generated at the San Diego Supercomputer Center and the Pittsburgh Supercomputer Center by SCEC modeling groups based at San Diego State University and Carnegie Mellon University. Intercomparisons of time series showed good agreement among the three groups.

[10] The low-frequency surface ground motions were saved on a 2-km grid covering a large portion of Southern California. For each of these 25,500 sites, the high-frequency motions were obtained following the method of *Graves and Pitarka* [2004]. This approach sums the response of each subfault assuming a random-phase, wavenumber-squared source spectrum with an amplitude level scaled to the subfault slip. We include both direct and Moho-reflected rays, which were traced through a 1D structure approximating the CVM4 average with gross impedance effects computed using quarter-wavelength theory [*Boore and Joyner*, 1997]. These simplified Green's functions were attenuated by a geometrical spreading factor computed as the inverse of the ray path length, a travel time-weighted Q operator, and a generic site spectral decay operator (kappa) of 0.04. The low frequency and high frequency results are combined using a set of matched filters with a cross over at 1 Hz.

[11] To account for site-specific geology, we applied frequency-dependent, non-linear amplification factors based on V_{s30}, the travel-time-weighted shear speed in the upper 30 m at the site. The site-specific V_{s30} values were taken from the map of *Wills et al.* [2000]. The form of the amplification factors were developed using equivalent linear site response analysis [*Walling et al.*, 2008] as implemented in the GMPE of *Campbell and Bozorgnia* [2008].

4. Simulation Results

[12] We processed the ground motion waveforms to extract peak ground acceleration (PGA), peak ground velocity (PGV), and 5% damped pseudo-spectral acceleration (SA) at a suite of oscillator periods. All metrics are computed for the geometric mean of the two horizontal components. Figure 2 displays maps of PGV for the three rupture scenarios. For ruptures of this magnitude, PGV tends to correlate with shaking periods in the range of 1–5 seconds, where the motions can be strongly influenced by rupture directivity and basin response. Ground motion maps for PGA and SA at periods of 0.3, 1.0 and 3.0 seconds, as

[1] Auxiliary materials are available in the HTML. doi:10.1029/2008GL035750.

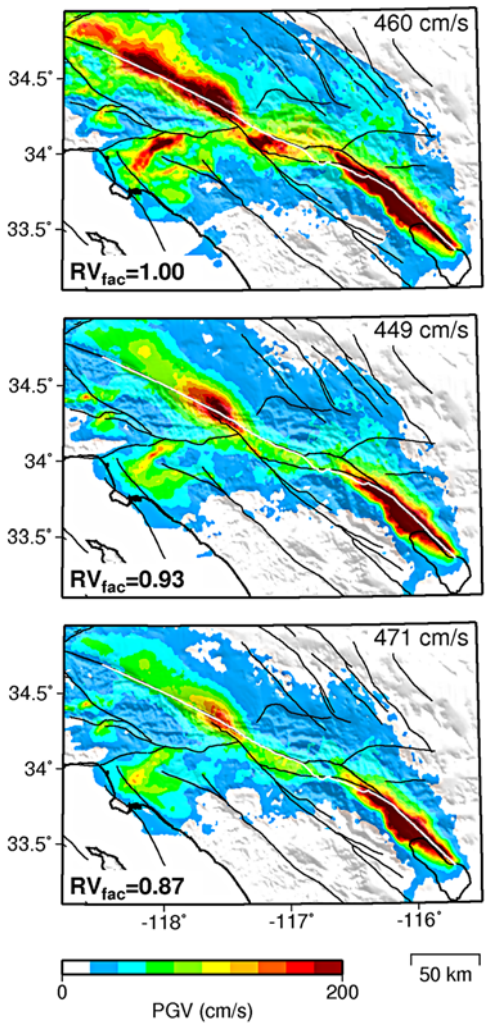

Figure 2. Maps of simulated peak ground velocity (PGV) for the three simulation scenarios. The largest value for each scenario is given in the upper right of each panel. Fault rupture trace is indicated by light grey line.

well as relative amplification maps, are provided in the auxiliary material.

[13] In all three scenarios the rupture begins at the southeast end of the fault and the wave energy is strongly focused to the northwest along the direction of fault rupture. However, the amplitude and spatial distribution of this directivity effect differs for the three rupture speed cases. The base case scenario (RV_{fac} = 1.00) generates the largest spatial extent of high amplitude near-fault motions with nearly the entire length of the fault exceeding 100 cm/s PGV. The slowest rupture speed case (RV_{fac} = 0.83) has the smallest region of high amplitude near-fault motions with only about half of the fault length exceeding the 100 cm/s level, primarily confined to the southern portion of the fault. However, this case predicts peak amplitudes along this section that are 30% higher than the base case.

[14] For these scenarios, the northward propagating wave energy is funneled westward into the string of sedimentary basins south of the San Gabriel Mountains—the San Bernardino, Chino, San Gabriel and Los Angeles basins—generating a very strong response in the Los Angeles region. This type of coupling between rupture directivity and basin amplification was first discovered in the TeraShake simulations of *Olsen et al.* [2006] based on kinematically prescribed fault rupture models. The phenomenon has also been confirmed using dynamic rupture models, although the inherent rupture complexity of the physically constrained dynamic sources reduces the basin response by factors of 2–3 in some locations [*Olsen et al.*, 2008]. Building upon this earlier work, our simulations show that the level of basin response is strongly influenced by rupture speed along the fault. The strongest basin response is generated in the base case scenario (RV_{fac} = 1.00) with PGV in the Whittier-Narrows corridor exceeding 200 cm/s. However, the level of basin response drops significantly as the rupture speed on the fault is decreased. The PGV in the Los Angeles region for the RV_{fac} = 0.87 case is about 50% less than the base case.

[15] Figure 3 displays ground velocity waveforms at three representative sites lying along the string of basins for the three rupture scenarios. Station **clt** is about 10 km from the fault in the San Bernardino basin, **rus** is in the Whittier-Narrows corridor at a fault distance of 49 km, and **dla** is over the deepest portion of the LA basin at a fault distance of 69 km (Figure 1). For **clt** and **rus**, the largest motions occur for the base case scenario, while for **dla** the largest motions occur for the lowest rupture speed case. These results highlight the complex nature of the interaction between source process effects and wave propagation effects at sites within these sedimentary basins. As the rupture speed is changed, the ground motion level at a particular site may increase or decrease depending on the strength of the radiated energy within a given frequency band and the relative coherence of the various phases that

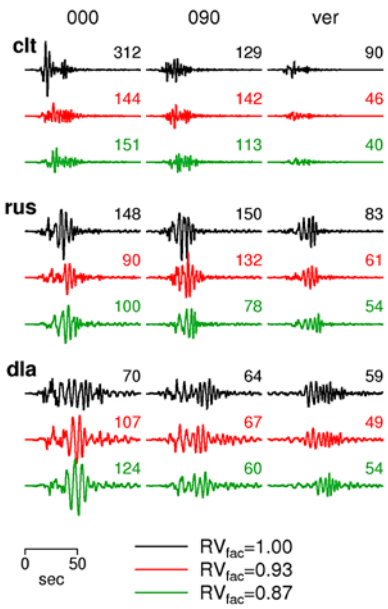

Figure 3. Three-component broadband ground velocity waveforms simulated at Colton (**clt**), Whittier-Narrows (**rus**) and Cerritos (**dla**) for each of the three scenarios. For each site, all traces are plotted on the same scale with the peak value (in cm/s) for each individual waveform shown above the trace.

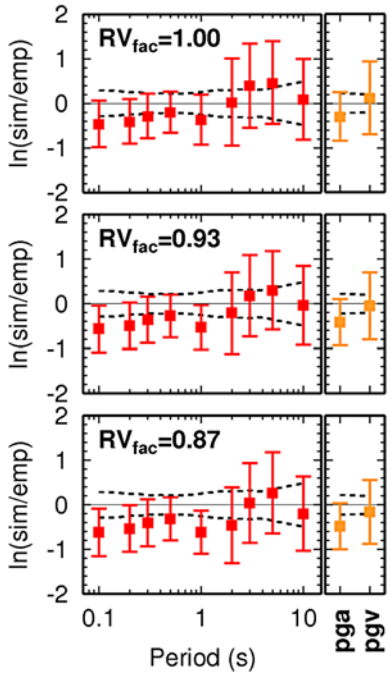

Figure 4. Average residuals between simulated SA, PGA and PGV and empirical estimates from the GMPE of *Campbell and Bozorgnia* [2008] for the three rupture scenarios. The error bars indicate one standard deviation for the residuals. The heavy dashed line represents one standard error of the inter-event term from the empirical model.

comprise the ground motion response. In addition, for deeper basin sites such as **dla**, multipathing effects can further modify the response. Wave field animations (www.shakeout.org/scenario) show that the later arriving phases in the deep basin are comprised of at least two distinct packets of wave energy; one that enters the basin to the south of the Puente Hills, and the other that enters from the north through the San Gabriel basin. The relative timing of these packets is sensitive to the rupture speed on the fault and in these scenarios, the lowest rupture speed case produces the strongest constructive interference in the region near **dla**. However, we must be careful not to generalize this result because this pattern would be sensitive to other factors not considered here, such as direction of rupture and relative geometry of the fault and basin margins.

5. Discussion and Conclusions

[16] Only a few strong motion recordings have been obtained for large magnitude (> 7.7) crustal earthquake ruptures, so it is difficult to directly compare our simulations with observed waveforms. One way to assess the simulations is to compare the computed shaking intensities with GMPE predictions, keeping in mind the GMPE represents a median expectation, whereas the simulation models the behavior for a single scenario having event-specific characteristics, and the GMPE, being based solely on observations, is poorly constrained for this type of rupture.

[17] Figure 4 shows the PGA, PGV and SA ratios between the medians from the simulations and the GMPE of *Campbell and Bozorgnia* [2008]. The trends seen in these residuals are generally consistent for the three scenarios: the simulations are at or below the GMPE estimates for SA periods less than 2 sec, and they are higher at periods of 3–5 sec. While this is not unexpected since the effects of directivity and basin response tend to be strongest in this bandwidth, another factor affecting the overall level of long-period ground motions in the simulations is fault slip. The median magnitude for our assumed fault rupture area predicted by the M_w-Area relation of *Somerville* [2006] is M_w 7.65. Our slip predictable model yields an M_w of 7.8, which requires about 70% more fault slip than the median event. Because the GMPE represents the median case, our simulated intensities may, in part, be larger at the long periods due to this effect.

[18] The median residuals shown in Figure 4 correspond to event terms, which express how the average ground motions from a particular event are offset from the GMPE median for the specified earthquake magnitude. The scatter of event terms observed from past earthquakes is reflected by the dotted lines in Figure 4. The scenario event terms are generally within one standard deviation, indicating the overall ground motion levels from the simulations are consistent with prior experience, and suggesting the simulated motions are neither unrealistic nor unprecedented. However, it appears that the simulated attenuation with distance may be too fast, which contributes to the negative bias of event terms for periods under 2–3 sec [*Star et al.*, 2008] (also see auxiliary material).

[19] We recognize that the kinematic ruptures used in these simulations represent just a few of the many potential ruptures that might occur along the southern San Andreas fault. Our finding that basin response can be strongly accentuated for ruptures propagating at or above the local shear wavespeed stresses the need for improved understanding of earthquake rupture physics. Ongoing studies using fully dynamic rupture simulations for ShakeOut-type events are providing valuable insight on the effects of source complexity on the level and variability of the resulting ground motions [*Olsen et al.*, 2008; S. Day et al., manuscript in preparation, 2008]. These studies may be particularly useful in providing constraints on allowable ranges of rupture speed and on possible correlations among parameters such as slip, rupture speed and rise time.

[20] **Acknowledgments.** We thank members of the SCEC CME collaboration for their efforts on the ShakeOut simulation project. We appreciate the constructive comments by Art Frankel, Paul Spudich and two anonymous reviewers. Funding for this work was provided by SCEC under NSF grants EAR-0623704 and OCI-0749313 and by the USGS. The large-scale simulations were run at USC's Center for High Performance Computing and Communications (http://www.usc.edu/hpcc) under an agreement with the SCEC CME project. This is SCEC contribution 1238.

References

Aagaard, B., and T. Heaton (2004), Near source ground motions from simulations of sustained intersonic and supersonic fault ruptures, *Bull. Seismol. Soc. Am.*, *94*, 2064–2078.

Aagaard, B., et al. (2008), Ground-motion modeling of the 1906 San Francisco earthquake, part II: Ground-motion estimates for the 1906 earthquake and scenario events, *Bull. Seismol. Soc. Am.*, *98*, 1012–1046.

Boore, D., and W. Joyner (1997), Site amplification for generic rock sites, *Bull. Seismol. Soc. Am.*, *87*, 327–341.

Campbell, K. W., and Y. Bozorgnia (2008), NGA ground motion model for the geometric mean horizontal component of PGA, PGV, PGD and 5% damped linear elastic response spectra for periods ranging from 0.01 to 10 s, *Earthquake Spectra*, *24*, 139–171.

Day, S. (1982), Three dimensional simulation of spontaneous rupture: The effect of non-uniform pre-stress, *Bull. Seismol. Soc. Am.*, *72*, 1881–1902.

Day, S., and C. Bradley (2001), Memory efficient simulation of anelastic wave propagation, *Bull. Seismol. Soc. Am.*, *91*, 520–531.

Freund, L. B. (1979), The mechanics of dynamic shear crack propagation, *J. Geophys. Res.*, *84*, 2199–2209.

Graves, R. (1996), Simulating seismic wave propagation in 3D elastic media using staggered grid finite differences, *Bull. Seismol. Soc. Am.*, *86*, 1091–1106.

Graves, R., and A. Pitarka (2004), Broadband time history simulation using a hybrid approach, paper presented at 13th World Conference on Earthquake Engineering, Can. Assoc. for Earthquake Eng., Vancouver, B. C., Canada.

Jones, L. M., et al. (2008), The ShakeOut xcenario, *U. S. Geol. Surv. Open File Rep., 2008–1150*. (Available at http://pubs.usgs.gov/of/2008/1150/)

Jordan, T. H., and P. Maechling (2003), The SCEC community modeling environment—An information infrastructure for system-level earthquake science, *Seismol. Res. Lett.*, *74*, 324–328.

Mai, M., and G. Beroza (2002), A spatial random field model to characterize complexity in earthquake slip, *J. Geophys. Res.*, *107*(B11), 2308, doi:10.1029/2001JB000588.

Olsen, K., S. Day, J. Minster, Y. Cui, A. Chourasia, M. Faerman, R. Moore, P. Maechlin, and T. Jordan (2006), Strong shaking in Los Angeles expected from a southern San Andreas earthquake, *Geophys. Res. Lett.*, *33*, L07305, doi:10.1029/2005GL025472.

Olsen, K. B., S. M. Day, J. B. Minster, Y. Cui, A. Chouasia, R. Moore, P. Maechling, and T. Jordan (2008), TeraShake2: Simulation of M_w 7.7 earthquakes on the southern San Andreas fault with spontaneous rupture description, *Bull. Seismol. Soc. Am.*, *98*, 1162–1185, doi:10.1785/0120070148.

Rosakis, A. J., O. Samudrala, and D. Coker (1999), Cracks faster than the shear wave speed, *Science*, *284*, 1337–1340.

Somerville, P. (2006), Review of magnitude-area scaling of crustal earthquakes, in *Report to 2007 WGCEP*, 22 pp., URS Corp., Pasadena, Calif.

Star, L. M., J. P. Stewart, R. W. Graves, and K. W. Hudnut (2008), Validation against NGA empirical model of simulated motions for *M*7.8 rupture of San Andreas fault, paper presented at 14th World Conference on Earthquake Engineering, China Earthquake Admin., Beijing, China.

Sieh, K., and P. Williams (1990), Behavior of the southernmost San Andreas fault during the past 300 years, *J. Geophys. Res.*, *95*, 6629–6645.

Walling, M., W. Silva, and N. Abrahamson (2008), Nonlinear site amplification factors for constraining the NGA models, *Earthquake Spectra*, *24*, 243–255.

Weldon, R. J., T. E. Fumal, G. P. Biasi, and K. M. Scharer (2005), Past and future earthquakes on the San Andreas fault, *Science*, *308*, 966–967.

Wills, C., M. Petersen, W. Bryant, M. Reichle, G. Saucedo, S. Tan, G. Taylor, and J. Treiman (2000), A site conditions map for California based on geology and shear wave velocity, *Bull. Seismol. Soc. Am.*, *90*, S187–S208.

B. T. Aagaard, USGS, 345 Middlefield Road, Menlo Park, CA 94025, USA.

R. W. Graves, URS Corporation, 566 El Dorado Street, Pasadena, CA 91101, USA. (robert_graves@urscorp.com)

K. W. Hudnut, USGS, 525 South Wilson Avenue, Pasadena, CA 91125, USA.

T. H. Jordan, Department of Earth Sciences, University of Southern California, Los Angeles, CA 90089, USA.

L. M. Star and J. P. Stewart, Department of Civil and Environmental Engineering, University of California, Los Angeles, CA 90095, USA.